MATHEMATICAL MODELLING OF CILIARY PROPULSION OF AN ELECTRICALLY-CONDUCTING JOHNSON-SEGALMAN PHYSIOLOGICAL FLUID IN A CHANNEL WITH SLIP

N. Manzoor [a] , O. Anwar Bég [b] , K. Maqbool* [a], S. Shaheen [a]

[a] Department of Mathematics & Statistics, International Islamic University, Islamabad 44000, Pakistan.

[b] Fluid Mechanics, Aeronautical/Mechanical Engineering, University of Salford, Manchester, M54WT, UK.

ABSTRACT: Bionic systems frequently feature electromagnetic pumping and offer significant advantages over conventional designs via intelligent bio-inspired properties. Complex wall features observed in nature also provide efficient mechanisms which can be utilized in biomimetic designs. The characteristics of biological fluids are frequently non-Newtonian in nature. In many natural systems super-hydrophobic slip is witnessed. Motivated by these phenomena, in the present article, we present a mathematical model for the cilia-generated propulsion of an electrically-conducting viscoelastic physiological fluid in a ciliated channel under the action of an externally applied static magnetic field. The rheological behavior of the fluid is simulated with the Johnson-Segalman constitutive model which allows internal wall slip. The regular or coordinated movement of the ciliated edges (which line the internal walls of the channel) is represented by a metachronal wave motion in the horizontal direction which generate a two-dimensional velocity profile with the parabolic profile in the vertical direction. This mechanism is imposed as a periodic moving velocity boundary condition which generates propulsion in the channel flow. Under the classical lubrication approximation (long wavelength and low Reynolds' number), the boundary value problem is rendered non-dimensional and solved analytically with a perturbation technique. The influence of the geometric, rheological (slip and Weissenberg number) and magnetic parameters on the velocity, pressure gradient and the pressure rise (evaluated via the stream function in symbolic software) are presented graphically and interpreted at length.

*Corresponding Author - Tel.: + 92 51-9019393 E-mail address: khadija.maqbool@iiu.edu.pk

NOMENCLATURE

$\overline{V}$	Velocity field vector
$\overline{U}, \overline{V}$	Longitudinal and transverse velocities in fixed frame

u, v	Longitudinal and transverse velocities in moving frame
$\overline{X}, \overline{Y}$	Coordinates of fixed frame
x, y	Coordinates of moving frame
μ	Dynamic viscosity of the fluid
f	Body force
B_0	Magnetic field
σ	Cauchy stress tensor
$\overline{P}$	Pressure
m	Relaxation time
ψ	Stream function
c	Wave speed
a	Rheological slip parameter
D	Symmetric of the velocity gradient
$\overline{w}$	Skew symmetric of the velocity gradient
M	Hartmann (magnetic body force) number
a_0	Wave amplitude
ε	Cilia length
α	Eccentricity of the elliptical motion
β	Wave number

1.INTRODUCTION

Cilia are membrane-bounded, centriole-derived projections which extend from the cell surface. They contain a microtubule cytoskeleton (the ciliary axoneme) engulfed by ciliary membrane. Many different types of cilia arise in human biology and their geometric design is critical to sustaining health [1-4]. Fluid transport induced by ciliary motion has therefore mobilized significant attention in biofluid dynamics for a number of decades. The initial hydrodynamic study of cilia beating was reported by Sleigh [5]. Numerous physiological processes feature ciliary transport including the movement of ovum in the fallopian tube [6], mucus transport in the respiratory track [7] spermatozoa dynamics in the ductus efferent of the male reproductive tract [8], spherule deposition during otolith formation in inner ear hydrodynamics [9] and molecular transport in photo-receptors for retinal bio-optics [10]. Cilia generate fluid transport via synchronized beating. When the cilia move, they transmit the energy to the fluid creating propulsion in the forward direction in the effective stroke. Naturally, the cilia are designed to move in hydrodynamically efficient ways. In the effective stroke cilia face large viscous resistance to generate the maximal thrust and in the recovery stroke they return to the initial position and the

cilia face small relative fluid velocities. Cilia groups (up to 200 cilia) exist on a mature ciliated cell, and each cilium is 1 to 10 µm long and of diameter around 0.2 µm, beats 12 to 15 times per second. The locomotion mechanism involves each cilium continuously moving or beating with a two-stroke motion, as visualized in **Fig.1**. Interestingly there are analogies between cilia beating and also aerodynamic flapping in small fliers (humming birds, bumble bees etc) which have been studied recently by Bég [11]. The cilia are closed together in rows and the neighboring cilia beat in a harmonized fashion manner with a small phase lag. In this way the tip of cilia are used to form a *continuous wave-like motion* termed the *metachronal wave* [12], similar to how continuous wing flapping in natural fliers generates a continuous lift force with very little energy expenditure. The fluid mechanism of cilia beating has been studied under various assumptions by many researchers [13-15] with the objective of characterizing the hydrodynamic characteristics which contribute to efficient propulsion. In the literature, there are two types of model for the propulsion and to transport fluid include: `cilia sublayer models' or `discrete cilia models' and volume force distribution' or `volume force models'. In the discrete cilia model, each cilium is treated separately, and the contributions of all the cilia are often summated [16]. In contrast, in volume force models the cilia are modelled through a continue force distribution, varying in space and times as the cilia beat [17]. In the present simulation, the envelope model is employed where only the tips of cilia are taken into account, and the tips are used to generate the so-called metachronal wave.

Magnetohydrodynamics (MHD) is an important area in modern smart (intelligent) bionic systems. It can be applied successfully to control flux, direction and other characteristics of the flow of electrically-conducting fluids. MHD features in numerous medical technologies e.g. MRI, GMR, EMG, IMF, etc wherein it allows the precise and non-invasive therapy of many physiological conditions. In biological propulsion, magnetohydrodynamic flows have been addressed for a variety of bionic systems including cliated magneto-hydraulics in soft robotics [18], respiratory magnetic treatment [19], peristaltic magnetofluid pumping [20-22], magnetic blood pumps [23-24], magneto-robotic microswimmers [25], cilia-assisted magnetic hemodynamic processes [26-28], biomagnetic curved arterial fluid mechanics [29].

Although the above studies considered many complex rheological fluids (viscoplastic, viscoelastic, two-phase, memory etc), they did not utilize the Johnson-Segalman non-Newtonian model. This model can simulate various physiological fluids quite well [30-32] and therefore the motivation of the present article is to investigate theoretically the influence of external (transverse)

magnetic field on the cilia transport of an electrically-conducting Johnson Segalman fluid in axisymmetric channel of finite length. In addition, we consider slip effects within the fluid (a feature which is included in the Johnson-Segalman model) since in numerous bionic microsystems non-adherence (slip) of the working fluid arises [33-37]. The paper is organized as follows. The governing problem is formulated as a nonlinear system of partial differential equations. These are simplified by applying the long wavelength and low Reynold number assumption [38]. With the aid of a perturbation method [39] the asymptotic solutions for axial velocity and axial pressure gradient are derived. Numerical integration of pressure rise is computed with the symbolic software, "MATHEMATICA". The effects of key parameters i.e. viscoelastic material parameter (Weissenberg number), cilia length, Hartmann (magnetic body force) number and hydrodynamic slip parameter on the flow characteristics are presented graphically. The simulations are relevant to bionic ciliated magnetic pumping systems.

2.MATHEMATICAL FORMULATION

Consider the flow of an incompressible magnetic Johnson-Segalman fluid through a symmetric ciliated channel of width *2L*, under the action of a transverse magnetic field, B_o. The *X*-axis is directed along the length of channel and in the direction of the metachronal wave. The model is depicted in **Fig. 1**.
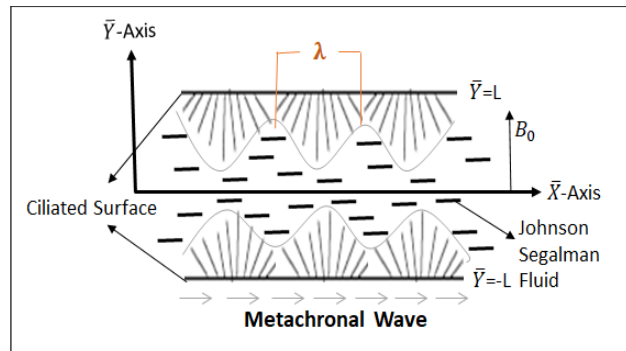
Fig.1: Geometry of Problem

Cilia are continuously beating with effective and recovery strokes and the tip of the cilia follow the elliptical path centered at ($\bar{X}_0, a_0$). The position of the cilia is given by the following parametric representation.

$$\overline{X} = F(\overline{X}, \overline{t}) = \overline{X}_0 + \varepsilon a_0 \alpha \sin\left(\frac{2\pi}{\lambda}\right)(\overline{X} - c\overline{t}) \tag{1}$$

$$\overline{Y} = H(\overline{X}, \overline{t}) = \pm\left[a_0 + \varepsilon a_0 \cos\left(\frac{2\pi}{\lambda}\right)(\overline{X} - c\overline{t})\right] = \pm L \tag{2}$$

Here $a_o \varepsilon \alpha$ is the major axis in the X-direction and $a_o \varepsilon$ is the minor axis in the Y-direction. After determining the location of the cilia tips, we may calculate the horizontal and vertical velocity components. The horizontal velocity $\overline{U}$ is obtained by the time derivative at $\overline{X}$ and vertical velocity $\overline{V}$ is calculated from the time derivative of vertical coordinate $\overline{Y}$ i.e.

$$\overline{U} = \frac{-\frac{2\pi}{\lambda}\left(\varepsilon a_0 \alpha \cos\left(\frac{2\pi}{\lambda}\right)(\overline{X} - c\overline{t})\right)}{1 - \frac{2\pi}{\lambda}\left(\varepsilon a_0 \alpha \cos\left(\frac{2\pi}{\lambda}\right)(\overline{X} - c\overline{t})\right)} \tag{3}$$

$$\overline{V} = \frac{-\frac{2\pi}{\lambda}\left(\varepsilon a_0 \sin\left(\frac{2\pi}{\lambda}\right)(\overline{X} - c\overline{t})\right)}{1 - \frac{2\pi}{\lambda}\left(\varepsilon a_0 \alpha \cos\left(\frac{2\pi}{\lambda}\right)(\overline{X} - c\overline{t})\right)} \tag{4}$$

Using the MHD Johnson-Segalman fluid model [40] the continuity and momentum equations in a fixed frame are defined as follows:

$$\operatorname{div}\overline{V} = 0, \tag{5}$$

$$\rho\frac{d\overline{V}}{d\overline{t}} = \operatorname{div}\overline{\sigma} + \rho\overline{f}, \tag{6}$$

Here:

$$\overline{\sigma} = -p\overline{I} + \overline{T}, \tag{7}$$

$$\overline{T} = 2\mu\overline{D} + \overline{S},$$

(8)

$$\overline{S} + m\left(\frac{d\overline{S}}{d\overline{t}} + \overline{S}\left(\overline{w} - a\overline{D}\right) + \left(\overline{w} - a\overline{D}\right)^{T}\overline{S}\right) = 2\eta\overline{D},$$

(9)

$$\overline{D} = \frac{1}{2}\left(\overline{L} + \overline{L}^{T}\right), \quad \overline{w} = \frac{1}{2}\left(\overline{L} - \overline{L}^{T}\right),$$
$$\overline{L} = \operatorname{grad}\overline{V}, \quad \overline{V} = \left(\overline{U}(x,y,t), \overline{V}(x,y,t), 0\right).$$

(10)

Eqns. (5) and (6) together with equations (7)-(10) take the following form:

$$\frac{\partial\overline{U}}{\partial\overline{X}} + \frac{\partial\overline{V}}{\partial\overline{Y}} = 0,$$

(11)

$$\rho\left(\frac{\partial\overline{U}}{\partial\overline{t}} + \overline{U}\frac{\partial\overline{U}}{\partial\overline{X}} + \overline{V}\frac{\partial\overline{U}}{\partial\overline{Y}}\right) = -\frac{\partial\overline{P}}{\partial\overline{X}} + \frac{\partial\overline{S}_{\overline{X}\overline{X}}}{\partial\overline{X}} + \frac{\partial\overline{S}_{\overline{X}\overline{Y}}}{\partial\overline{Y}} - \sigma B_0^2\overline{U},$$

(12)

$$\rho\left(\frac{\partial\overline{V}}{\partial\overline{t}} + \overline{U}\frac{\partial\overline{V}}{\partial\overline{X}} + \overline{V}\frac{\partial\overline{V}}{\partial\overline{Y}}\right) = -\frac{\partial\overline{P}}{\partial\overline{Y}} + \frac{\partial\overline{S}_{\overline{X}\overline{Y}}}{\partial\overline{X}} + \frac{\partial\overline{S}_{\overline{Y}\overline{Y}}}{\partial\overline{Y}},$$

(13)

Here $\overline{S}_{\overline{X}\overline{X}}, \overline{S}_{\overline{X}\overline{Y}}$ and $\overline{S}_{\overline{Y}\overline{Y}}$ satisfy following equations:

$$2\eta\frac{\partial\overline{U}}{\partial\overline{X}} = \overline{S}_{\overline{X}\overline{X}} + m\left(\overline{U}\frac{\partial}{\partial\overline{X}} + \overline{V}\frac{\partial}{\partial\overline{Y}}\right)\overline{S}_{\overline{X}\overline{X}} - 2am\overline{S}_{\overline{X}\overline{X}}\frac{\partial\overline{U}}{\partial\overline{X}}$$
$$+ m\left((1-a)\frac{\partial\overline{V}}{\partial\overline{X}} - (1+a)\frac{\partial\overline{U}}{\partial\overline{Y}}\right)\overline{S}_{\overline{X}\overline{Y}},$$

(14)

$$\eta\left(\frac{\partial \overline{U}}{\partial \overline{Y}}+\frac{\partial \overline{V}}{\partial \overline{X}}\right)=\overline{S}_{XY}+m\left(\overline{U}\frac{\partial}{\partial \overline{X}}+\overline{V}\frac{\partial}{\partial \overline{Y}}\right)\overline{S}_{XY}$$
$$+\frac{m}{2}\left((1-a)\frac{\partial \overline{U}}{\partial \overline{Y}}-(1+a)\frac{\partial \overline{V}}{\partial \overline{X}}\right)\overline{S}_{XX}$$
$$+\frac{m}{2}\left((1-a)\frac{\partial \overline{V}}{\partial \overline{X}}-(1+a)\frac{\partial \overline{U}}{\partial \overline{Y}}\right)\overline{S}_{YY},$$

(15)

$$2\eta\frac{\partial \overline{V}}{\partial \overline{Y}}=\overline{S}_{YY}+m\left(\overline{U}\frac{\partial}{\partial \overline{X}}+\overline{V}\frac{\partial}{\partial \overline{Y}}\right)\overline{S}_{YY}-2am\overline{S}_{YY}\frac{\partial \overline{V}}{\partial \overline{Y}}$$
$$+m\left((1-a)\frac{\partial \overline{U}}{\partial \overline{Y}}-(1+a)\frac{\partial \overline{V}}{\partial \overline{X}}\right)\overline{S}_{XY}.$$

(16)

The fixed and the wave frame are related as:

$$\overline{x}=\overline{X}-c\overline{t},\quad \overline{y}=\overline{Y},\quad \overline{u}=\overline{U}-c,\quad \overline{v}=\overline{V},$$
$$\overline{p}(\overline{x},\overline{y},\overline{t})=\overline{P}(\overline{X},\overline{Y},\overline{t}),$$

(17)

The non-dimensional variables are defined as follows:

$$x=\frac{\overline{X}}{\lambda},\quad y=\frac{\overline{Y}}{a},\quad u=\frac{\overline{u}}{c},\quad v=\frac{\lambda\overline{v}}{ac},\quad t=\frac{c\overline{t}}{\lambda},$$
$$\beta=\frac{a_0}{\lambda},h=\frac{L}{a},\ S_{ij}=\frac{a}{\mu c}\overline{S}_{ij},\ p=\frac{a_0^2}{\lambda(\mu+\eta)}\overline{p},$$
$$M^2=\frac{\sigma B_0^2 a_0^2}{\mu},\quad We=\frac{mc}{a_0},\quad Re=\frac{\rho c a_0}{\mu}.$$

(18)

Here β is wave number, M is Hartmann magnetic number, Re is the Reynolds number and We is the Weissenberg number. Since the flow is incompressible and two-dimensional, a natural formulation is obtained by introducing the stream function, ψ, defined by the Cauchy-Riemann equations:

$$u = \frac{\partial \psi}{\partial y} \qquad v = -\frac{\partial \psi}{\partial y}.$$

(19)

With the help of Eqns. (17)-(19) and the lubrication approximations (long wavelength relative to channel width and low Reynolds number), Eqns. (11)-(16) take the following form:

$$\left(\frac{\mu + \eta}{\mu}\right)\frac{\partial p}{\partial x} = \frac{\partial S_{xy}}{\partial y} + \frac{\partial^3 \psi}{\partial y^3} - M^2\left(\frac{\partial \psi}{\partial y} + 1\right)$$

(20)

$$\frac{\partial p}{\partial y} = 0,$$

(21)

$$S_{xx} = We(1 + a)\frac{\partial^2 \psi}{\partial y^2}S_{xy},$$

(22)

$$\frac{\eta}{\mu}\frac{\partial^2 \psi}{\partial y^2} = S_{xy} + \frac{We}{2}(1 - a)\frac{\partial^2 \psi}{\partial y^2}S_{xx} - \frac{We}{2}(1 + a)\frac{\partial^2 \psi}{\partial y^2}S_{yy},$$

(23)

$$S_{yy} = -We(1 - a)\frac{\partial^2 \psi}{\partial y^2}S_{xy}.$$

(24)

After using Eqn. (21) in Eqn. (20), following expression can be obtained:

$$\frac{\partial^2 S_{xy}}{\partial y^2} + \frac{\partial^4 \psi}{\partial y^4} - M^2\frac{\partial^2 \psi}{\partial y^2} = 0.$$

(25)

From Eqns. (22)-(24), the shear stress, S_{xy}, can be found as follows:

$$S_{xy} = \frac{\frac{\eta}{\mu}\frac{\partial^2 \psi}{\partial y^2}}{1 + We^2(1 - a^2)\left(\frac{\partial^2 \psi}{\partial y^2}\right)^2}.$$

(26)

Now substituting Eqn. (26) into Eqns. (25) and (20) yields:

$$\frac{\partial^2}{\partial y^2}\left(\frac{\left(\frac{\eta}{\mu}+1\right)\frac{\partial^2\psi}{\partial y^2}+We^2(1-a_0^2)\left(\frac{\partial^2\psi}{\partial y^2}\right)^3}{1+We^2(1-a^2)\left(\frac{\partial^2\psi}{\partial y^2}\right)^2}-M^2\psi\right)=0,$$

(27)

$$\left(\frac{\mu+\eta}{\mu}\right)\frac{\partial p}{\partial x}=\frac{\partial}{\partial y}\left(\frac{\frac{\eta}{\mu}\frac{\partial^2\psi}{\partial y^2}}{1+We^2(1-a^2)\left(\frac{\partial^2\psi}{\partial y^2}\right)^2}\right)+\frac{\partial^3\psi}{\partial y^3}$$

$$-M^2\left(\frac{\partial\psi}{\partial y}+1\right)=0,$$

(28)

3. VOLUMETRIC FLOW RATE AND BOUNDARY CONDITIONS

In bionic pumping systems, flow rate is a key design quantity. The volume flow rate Q is related to the flux F by the following relation:

$$Q=\int_0^h\left(\frac{\partial\psi}{\partial y}+1\right)dy=F+h,$$

(29)

Another physical quantity is the time-mean volume flow rate, $\bar{Q}$, in a fixed frame which is defined as:

$$\bar{Q}=\frac{1}{T}\int_0^h(F+h)d\bar{t}=\int_0^1(F+h)dt=F+1,$$

(30)

If we choose the zero value of the streamline ($y = 0$), as $\psi = 0$, then the wall ($y = h$) is the streamline of value $\psi = F$. Thus, the boundary conditions in the form of stream function ψ are

$$\psi=0,\quad\frac{\partial^2\psi}{\partial y^2}=0,\quad\text{at }y=0,$$

(31)

$$\psi=F,\quad\frac{\partial\psi}{\partial y}=-1-2\pi\varepsilon\alpha\beta\cos\left(2\pi x\right),$$

$$\text{at }y=h=1+\varepsilon\sin\left(2\pi x\right).$$

(32)

With the help of binomial theorem, we neglect higher powers of $\left(\frac{\partial^2\psi}{\partial y^2}\right)$ i.e. $o\left(\frac{\partial^2\psi}{\partial y^2}\right)^6$. Eqns. (27) and (28) then take the following form:

$$\frac{\partial^2}{\partial y^2}\left(\frac{\partial^2\psi}{\partial y^2} + We^2\kappa_2\left(\frac{\partial^2\psi}{\partial y^2}\right)^3 - \kappa_1 M^2\psi\right) = 0,$$

(33)

$$\frac{\partial p}{\partial x} = \frac{\partial}{\partial y}\left(\frac{\partial^2\psi}{\partial y^2} + We^2\kappa_2\left(\frac{\partial^2\psi}{\partial y^2}\right)^3\right) - \kappa_1 M^2\left(\frac{\partial\psi}{\partial y} + 1\right),$$

(34)

Here:

$$\kappa_1 = \frac{\mu}{\mu + \eta}, \quad \kappa_2 = \frac{(a^2 - 1)\eta}{\eta + \mu}.$$

(35)

Here μ, η are viscosity coefficients of the Johnson-Segalman fluid, a is slip parameter.

4. PERTURBATION SOLUTIONS

To solve the non-linear Eqns. (33) and (34) together with the boundary condition (31) and (32), a perturbation method is employed. Expanding the stream function ψ, pressure distribution p and flow rate F about the Weissenberg number We (assuming small Weissenberg number) leads to:

$$\psi = \psi_0 + We^2\psi_1 + ...,$$

(36)

$$p = p_0 + We^2 p_1 + ...,$$

(37)

$$F = F_0 + We^2 F_1 + ...,$$

(38)

Using the above equations in (34)-(36) we get the following systems:

4.1 Zeroth Order System

$$\frac{\partial^2}{\partial y^2}\left(\frac{\partial^2\psi_0}{\partial y^2} - M^2\left(\frac{\mu}{\mu+\eta}\right)\psi_0\right) = 0,$$

(39)

$$\frac{dp_0}{dx} = \frac{\partial}{\partial y}\left(\frac{\partial^2\psi_0}{\partial y^2}\right) - M^2\left(\frac{\mu}{\mu+\eta}\right)\left(\frac{\partial\psi_0}{\partial y} + 1\right),$$

(40)

The associated boundary conditions are:

$$\psi_0 = 0, \quad \frac{\partial^2\psi_0}{\partial y^2} = 0, \quad \text{at } y = 0,$$

(41)

$$\psi_0 = F_0, \quad \frac{\partial\psi_0}{\partial y} = -1 - 2\pi\varepsilon\alpha\beta\cos\left(2\pi x\right),$$
$$\text{at } y = h = 1 + \varepsilon\sin\left(2\pi x\right),$$

(42)

4.2 First order system

$$\frac{\partial^2}{\partial y^2}\left(\frac{\partial^2\psi_1}{\partial y^2} + \frac{(a^2-1)\eta}{\eta+\mu}\left(\frac{\partial^2\psi_1}{\partial y^2}\right)^3 - M^2\left(\frac{\mu}{\mu+\eta}\right)\psi_1\right) = 0,$$

(43)

$$\frac{\partial p_1}{\partial x} = \frac{\partial}{\partial y}\left(\frac{\partial^2\psi_1}{\partial y^2} + \frac{(a^2-1)\eta}{\eta+\mu}\left(\frac{\partial^2\psi_1}{\partial y^2}\right)^3\right)$$
$$- M^2\left(\frac{\mu}{\mu+\eta}\right)\left(\frac{\partial\psi_1}{\partial y} + 1\right),$$

(44)

The relevant boundary conditions are:

$$\psi_1 = 0, \quad \frac{\partial^2\psi_1}{\partial y^2} = 0, \quad \text{at } y = 0,$$

(45)

$$\psi_1 = F_1, \quad \frac{\partial \psi_1}{\partial y} = 0, \quad \text{at} \ \ y = h = 1 + \varepsilon \sin\left(2\pi x\right),$$

(46)

4.3 Solution for the Zeroth order system

The solution of the zeroth order system given by Eqns. (39)-(42) is as follows:

$$\psi_0 = \frac{\begin{array}{c}-MyCosh(Mh\sqrt{\kappa_1})F_0\sqrt{\kappa_1} + ySinh(Mh\sqrt{\kappa_1})u_0 \\ +Sinh(My\sqrt{\kappa_1})(F_0 - hu_0)\end{array}}{Sinh(Mh\sqrt{\kappa_1}) - MCosh(Mh\sqrt{\kappa_1})h\sqrt{\kappa_1}},$$

(47)

With the help of Eqns. (40) and (47), the *zeroth order pressure gradient* can be obtained:

$$\frac{dp_0}{dx} = \frac{\begin{array}{c}M^2\kappa_1(-MCosh(Mh\sqrt{\kappa_1})(h + F_0)\sqrt{\kappa_1}) \\ +Sinh(Mh\sqrt{\kappa_1})(1 + u_0))\end{array}}{-Sinh(Mh\sqrt{\kappa_1}) + MCosh(Mh\sqrt{\kappa_1})h\sqrt{\kappa_1}}.$$

(48)

4.4 Solution for the First order system

Solving the first order system as given by Eqns. (43)-(46), we obtain:

$$\psi_1 = \frac{1}{64((Sinh(Mh\sqrt{\kappa_1}) - MCosh(Mh\sqrt{\kappa_1})h\sqrt{\kappa_1}))^4}$$
$$[(8F_1(8Sinh(My\sqrt{\kappa_1})(Sinh[Mh\sqrt{\kappa_1}))^3$$
$$+M\sqrt{\kappa_1}(-8yCosh(Mh\sqrt{\kappa_1})(Sinh(Mh\sqrt{\kappa_1}]^3$$
$$+h(-3(Sinh(M(y - 3h)\sqrt{\kappa_1}) - Sinh(M(y - h)\sqrt{\kappa_1})$$
$$-Sinh(M(y + h)\sqrt{\kappa_1}) + Sinh(M(y + 3h)\sqrt{\kappa_1}))$$
$$+M\sqrt{(\kappa_1)}(6y(Sinh(2Mh\sqrt{\kappa_1})^2 + h(-3(Cosh(M(y - 3h)\sqrt{\kappa_1})$$
$$+Cosh(M(y - h)\sqrt{\kappa_1}) - Cosh(M(y + h)\sqrt{\kappa_1})$$
$$-Cosh(M(y + 3h)\sqrt{\kappa_1})) - 8M(Cosh(Mh\sqrt{\kappa_1}))^3(hSinh(My\sqrt{\kappa_1})$$
$$+3ySinh(Mh\sqrt{\kappa_1}))\sqrt{\kappa_1} + 8M^2y(Cosh(Mh\sqrt{\kappa_1}))^4h\kappa_1)))))$$
$$-M^4\kappa_1)^2(-Cosh(M(y - 3h)\sqrt{\kappa_1}) + Cosh(M(3y - h)\sqrt{\kappa_1})$$
$$-Cosh(M(3y + h)\sqrt{\kappa_1}) + Cosh(M(y + 3h)\sqrt{\kappa_1})$$
$$+M(2y(-6Sinh(M(y - h)\sqrt{\kappa_1}) - 8Sinh(2Mh\sqrt{\kappa_1})$$
$$+Sinh(4Mh\sqrt{\kappa_1}) + 6Sinh(M(y + h)\sqrt{\kappa_1}))$$
$$+h(-3Sinh(M(y - 3h)\sqrt{\kappa_1}) + Sinh(M(3y - h)\sqrt{\kappa_1})$$
$$+Sinh(M(3y + h)\sqrt{\kappa_1}) - 3Sinh(M(y + 3h)\sqrt{\kappa_1})))\sqrt{\kappa_1}$$
$$+24M^2h(y - yCosh(My\sqrt{(\kappa_1)})Cosh(Mh\sqrt{\kappa_1})$$
$$+hSinh(My\sqrt{\kappa_1})Sinh(Mh\sqrt{\kappa_1}))\kappa_1)\kappa_2((-F_0 + hu_0))^3)],$$

(49)

Substituting Eqn. (49) into Eqn. (44), we arrive at the *first order pressure gradient:*

$$
\begin{aligned}
\frac{dp_1}{dx} = &\frac{1}{(32((Sinh(Mh\sqrt{\kappa_1}) - MCosh(Mh\sqrt{\kappa_1})h\sqrt{\kappa_1})^4)} \\
&[(M^2\kappa_1(-16Cosh(2Mh\sqrt{\kappa_1})(-1 + M^4h^3(h + F_1)\kappa_1^2) \\
&-4Cosh(4Mh\sqrt{\kappa_1})(1 + M^2h\kappa_1(3F_1 + h(6 + M^2h(h + F_1)\kappa_1)))) \\
&-8MSinh(2Mh\sqrt{\kappa_1})\sqrt{\kappa_1}(F_1 - M^4F_0^3\kappa_1^2\kappa_2 + h(4 + 3M^4F_0^2\kappa_1^2\kappa_2u_0) \\
&-3M^2h^2\kappa_1(F_1 + M^2F_0\kappa_1\kappa_2u_0^2) + M^2h^3\kappa_1(-4 + M^2\kappa_1\kappa_2u_0^3)) \\
&+MSinh(4Mh\sqrt{\kappa_1})\sqrt{\kappa_1}(4F_1 - M^4F_0^3\kappa_1^2\kappa_2 + h(16 + 3M^4F_0^2\kappa_1^2\kappa_2u_0) \\
&-3M^2h^2\kappa_1(-4F_1 + M^2F_0\kappa_1\kappa_2u_0^2) + M^2h^3\kappa_1(16 + M^2\kappa_1\kappa_2u_0^3)) \\
&+12(-1 + M^2h\kappa_1(F_1 - M^4F_0^3\kappa_1^2\kappa_2 + h(2 + 3M^4F_0^2\kappa_1^2\kappa_2u_0) \\
&-M^2h^2\kappa_1(F_1 + 3M^2F_0\kappa_1\kappa_2u_0^2) + M^2h^3\kappa_1(-1 + M^2\kappa_1\kappa_2u_0^3))))))].(50)
\end{aligned}
$$

Now summarize the above results up to order We^2 and to achieve the final results to introduce $F = F_0 + We^2 F_1$ or $F_0 = F\text{-}We^2 F_1$ in the stream function ψ and pressure gradient $\frac{dp}{dx}$ given in Eq. (36) and (37). Where ψ_o and ψ_1, $\frac{dp_0}{dx}$ and $\frac{dp_1}{dx}$ are defined in Eqns. (47)-(50).

5. RESULTS AND DISCUSSION

Figs. 2, 3 and 4 are plotted to visualize the effects of the key parameters i.e. Hartmann number, Weissenberg number, slip parameter and the cilia length, on the velocity, pressure and the pressure rise, keeping all other parameter fixed.

Figs. 2a-2d illustrate the impact of *Hartmann number (M), Weissenberg number (We), slip parameter (a) and cilia length (ε) on the axial pressure (p) evolution with axial coordinate (x) i.e. pressure gradient.* Fig. 2a shows that pressure is strongly modified by the Hartmann number. With increasing Hartmann number there is a uniform decrease in pressure. A reduction in pressure is also induced with increasing slip parameter in fig 2c. However pressure is boosted with elevation in Weissenberg number (fig. 2c) and cilia length (fig. 2d). There is a more uniform pressure distribution along the channel length with variation in Hartmann number (fig. 2a) and the principal reduction in pressure is concentrated in the intermediate section of the channel; lower pressures arise at the entry and exit of the channel with maximum pressures in between, an important feature

required for efficient medical magnetic pump performance [41].
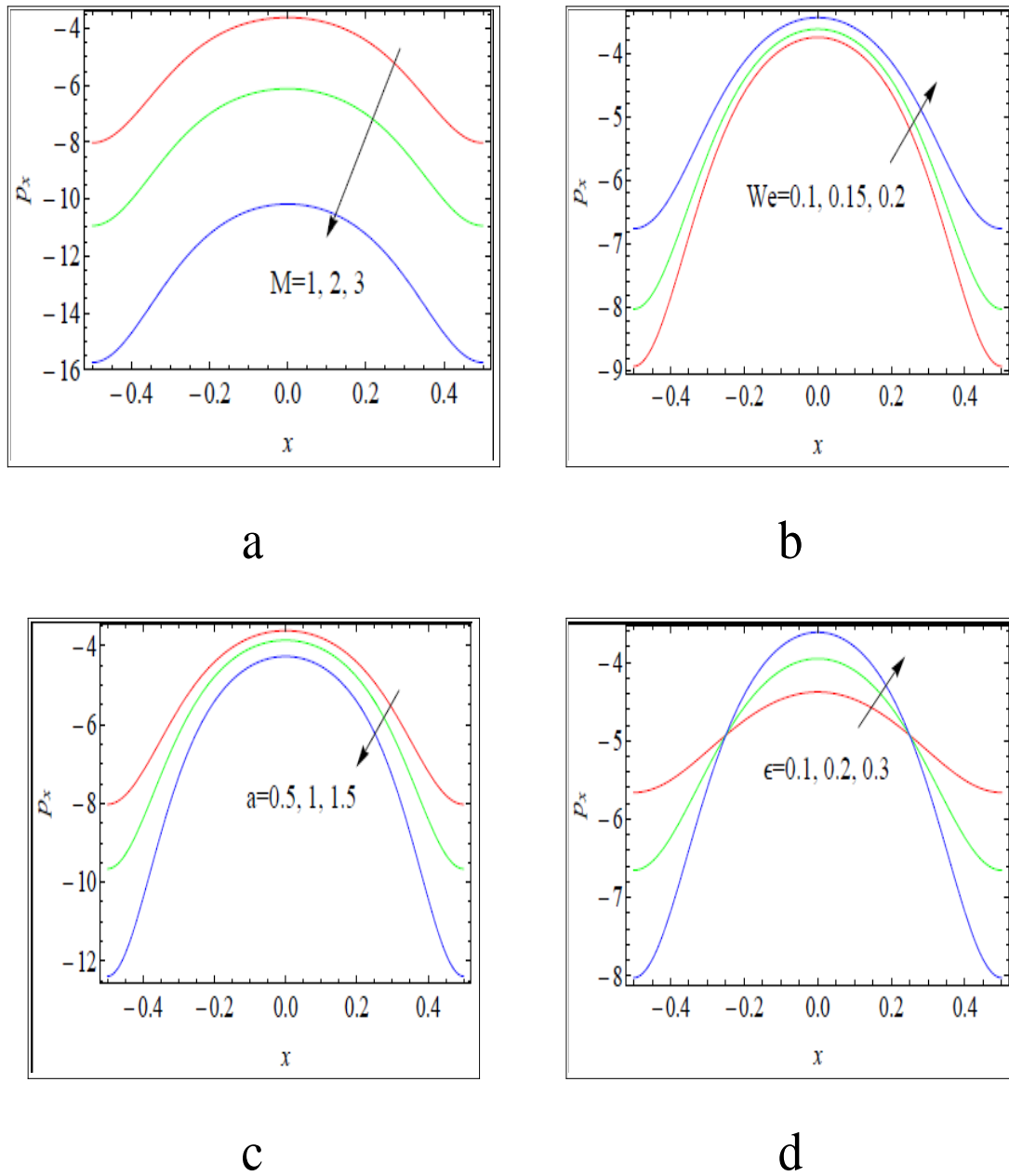
Fig. 2: Axial pressure distributions with variation in (*a*) *Hartmann number   (M), (b) Weissenberg number (We), (c) Slip parameter (a), (d) Cilia length (ε) , for α=0.4, β=0.4, μ=1, η=1,Q^{----}=1.5.*
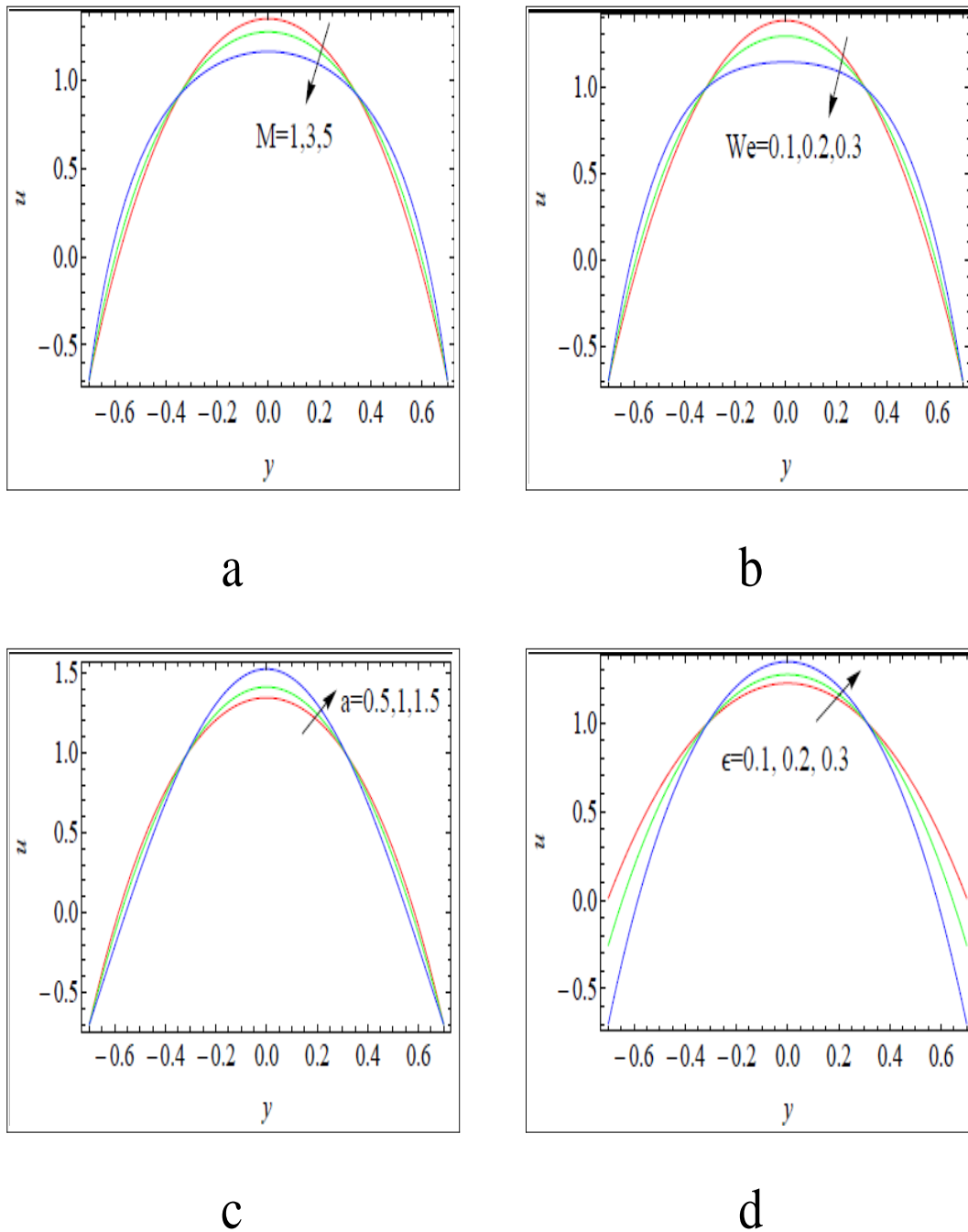
Fig. 3: Axial velocity distributions across channel span with variation in (*a*) *Hartmann number (M), (b) Weissenberg number (We), (c) Slip parameter (a), (d) Cilia length (ε), for α=0.4, β=0.4, μ=1, η=1,$\overline{Q}$=1.5.*

a

b

c

d
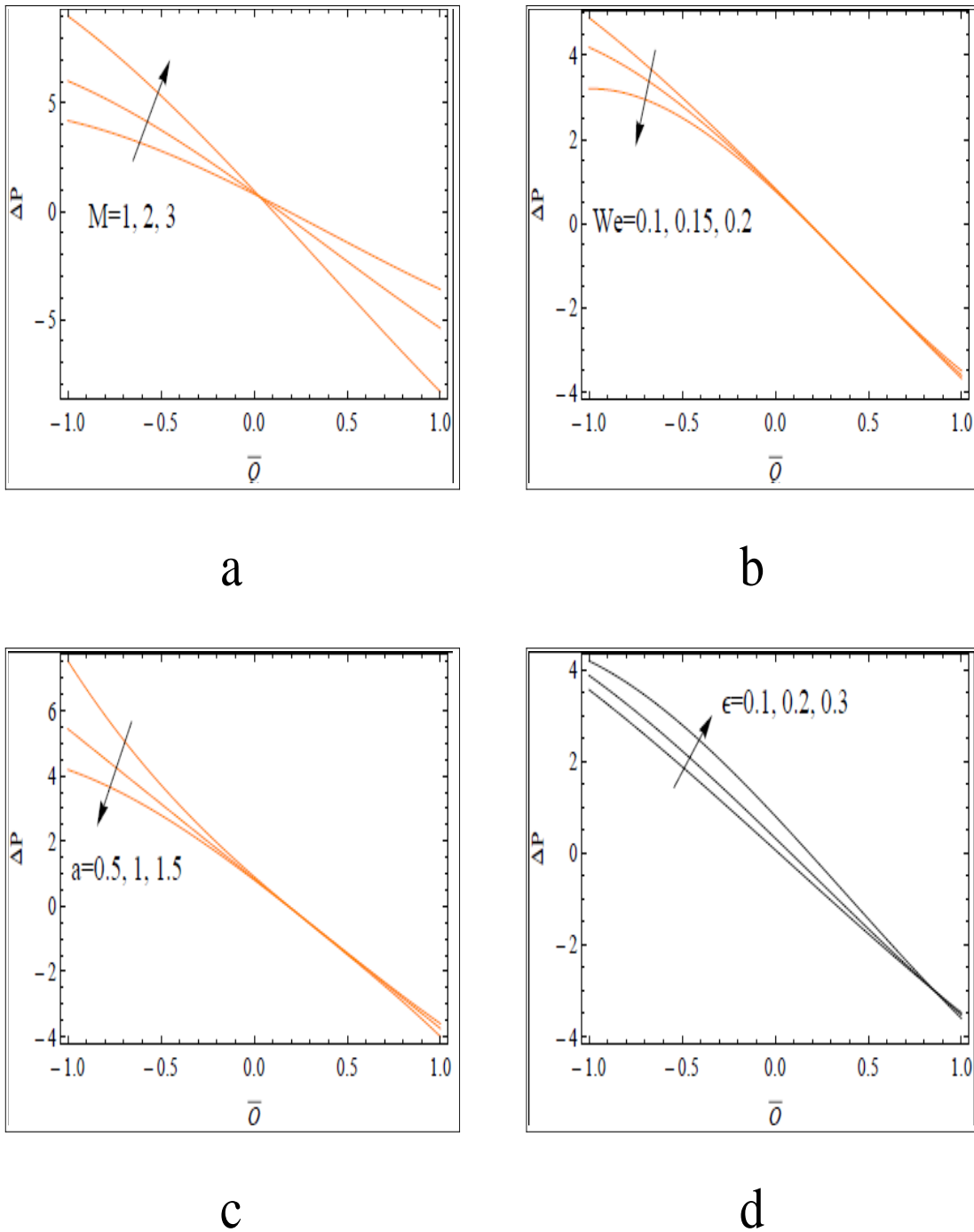
Fig. 4: Axial velocity distributions versus average volumetric flow rate with variation in (*a*) *Hartmann number (M), (b) Weissenberg number (We), (c) Slip parameter (a), (d) Cilia length (ε), for α=0.4, β=0.4, μ=1, η=1,Q̄=1.5.*

Hartmann number appears in the Lorentz magnetohydrodynamic body force terms in Eqns. (33) and (34). This is a retarding force which opposes the flow and induces deceleration across the channel span (described later). Effectively pressure is suppressed with stronger magnetic field. The maximum pressure is achieved for the case $M = 1$ wherein magnetic and viscous forces in the regime are equivalent in magnitude. For $M > 1$ the magnetic drag force dominates the viscous hydrodynamic resistance. Figs. 2b-d indicate that the other parameters induce a more marked modification in pressure profiles in the vicinity of the entry and exit zones (low and high values of axial coordinate). The viscoelastic parameter i.e. Weissenberg number embodies the relative contribution of viscous forces to the elastic forces and describes mathematically the relationship between stress relaxation time of the fluid and a specific process time. For cases where the time-scale of a flow is significantly less than the relaxation time of the viscoelastic fluids, then elastic effects dominate the flow behavior. However, when time-scale exceeds the relaxation time, substantial elastic relaxation takes place and the viscous forces dominate the flow. The Johnson-Segalman fluid model is more sophisticated than other viscoelastic models and permits the nonmonotonic variation in the shear stress with the increase/decrease in the rate of deformation for simple shear flows. It is also capable of simulating slip effects and furthermore the spurt phenomenon [42] i.e. an abnormal increase in the volume throughput for a very weak elevation in the driving pressure gradient. With greater Weissenberg numbers the elastic effect dominates the behavior and this contributes to the enhancement in pressure. This has also been observed by other investigators including Hayat *et al.* [43] and Elshahed and Haroun [44]. With greater slip effect the pressure is decreased significantly (Fig. 2c). The increase in pressure with greater cilia length is related to the enhanced transfer of force to the fluid in the channel with larger cilia geometry. This boosts the pressure in the central channel length area but depresses the pressure near the entry and exit locations.

Figs. 3a-3d illustrate the influence of the key parameters on the axial velocity across the channel span i.e. with transverse coordinate, *y*. Evidently although symmetrical profiles in velocity are consistently computed, the parameters exhibit different effects. Fig. 3a and 3b show that velocity decreases with the increase in Hartmann number and Weissenberg number *in the central (core) region, -0.32<y<0.32* and increases near the walls in the range, y<-0.32 and y>0.32 of the channel. The contrary behavior can be observed with an increase in slip parameter and cilia length from Figs. 3c and 3d. Furthermore, inspection of the figures reveals that Hartmann number,

Weissenberg number and slip parameter generate a more significant influence at the centre as compared to walls of the channel.

The expression for the *pressure rise* is:

$$\triangle p = \int_0^1 \frac{dp}{dx} dx,$$

(51)

To calculate the result of volume flow rate, we use the expression of Δp which involves the integration of *dp/dx*. Due to the complexity of the expression given in the Eq. (51), the symbolic software, MATHEMATICA, has been implemented for the numerical integration. The results are shown in Figs. 4a-4b, which present the evolution in average rise in the pressure against $\bar{Q}$ (time-averaged flux). The effect of Hartmann number (M) on pressure rise depicted in Fig. 4a, which shows the retrograde pumping ($\bar{Q}<0$, Δp>0) and the free pumping ($\Delta p=0$) uniformly change with the increase in Hartmann number. Fig. 4b and 4c, reveals the variation of pressure rise against time average flux, for the different value of Weissenberg number, *We* and the slip parameter, *a*. It is noted that co-pumping rate decreases with an increase in Weissenberg number and the slip parameter. Fig. 4d, shows the effect of cilia length (ε) on the pressure rise. It is evident that the pumping and the co-pumping rates increases with an increase in cilia length.

6. CONCLUSIONS

In this study, we have considered the ciliary transport of MHD Johnson-Segalman fluid in a two-dimensional symmetric channel. The flow is produced by the continuous beating of cilia in an elliptical path which generates the two-dimensional velocity field. The governing equations are simplified by using lubrication theory and converted into non-dimensional form via suitable transformations. A regular perturbation technique is used to solve the non-linear partial differential equations with appropriate boundary conditions. Mathematica symbolic software is deployed to evaluate the closed-form solutions and results are visualized graphically. The principal findings from the present study may be summarized as follows:

- The pressure gradient is strongly affected by the Weissenberg viscoelastic number (*We*) and cilia length (ε).

- With the increase in Weissenberg viscoelastic number (*We*) and cilia length (ε) larger pressure gradient is required to maintain the same flux through a narrow region as compared to a wider

region of channel, whereas, smaller pressure gradient is required with an increase in Hartmann magnetic parameter (M) and slip parameter (a).

- The velocity response is not the same throughout the channel- velocity decreases in the narrow region with an increase in Hartmann magnetic number (M) and Weissenberg number (We) whereas it increases with a rise in slip parameter (a) and cilia length (ε).

- Pressure rise increases with an increase in Hartmann magnetic number (M) and cilia length (ε) whereas it is reduced with greater values of Weissenberg number (We) and cilia length (ε).

The present investigation has neglected *curvature, rotational and heat transfer* effects which are also important in biomimetic pumps [45] and these may be addressed in the future.

REFERENCES

[1] Blake, J. (1973). Flow in tubules due to ciliary activity. *Bulletin Mathematical Biology,* 35, 513-523.

[2] Brennen, C. (1974). An oscillating-boundary-layer theory for ciliary propulsion, *J. Fluid Mech*. 65, 799-824.

[3] Maqbool, K., S. Shaheen and A.B. Mann (2016). Exact solution of cilia induced flow of a Jeffrey fluid in an inclined tube, *SpringerPlus,* 5, 1379-1395.

[4] Sadiqui, A. M., A. A. Farooq and M. A. Rana (2014). Hydromagnetic flow of Newtonian fluid due to ciliary motion in the channel. *Magnetohydrodynamics,* 50, 109-122.

[5] Sleigh, M. A. (1962). *The Biology of Cilia and Flagella* (MacMillan, New York, USA).

[6] Sturgis, S. H. (1947). The effect of ciliary current on sperm progress in excised human fallopian tubes. *Trans. Amer. Soc. Study Sterility* 3, 31-39.

[7] Wanner, A., M. Salathé and T. G. O'Riordan (1996). Mucociliary clearance in the airways. *American Journal Respiratory Critical Care Medicine* 154, 1868-1902.

[8] Lardner, T. J. and W. J. Shack (1972). Cilia transport. *Bulletin Mathematical Biophysics*, 34(3), 325-335.

[9] J.R. Colantonio *et al.* (2009). The dynein regulatory complex is required for ciliary motility and otolith biogenesis in the inner ear. *Nature*. 2009; 457: 205–209.

[10] Horst, C. J., Johnson, L. V. and Besharse, J. C. (1990). Transmembrane assemblage of the photoreceptor connecting cilium and motile cilium transition zone contain a common immunologic

epitope, *Cell Motil. Cytoskeleton,* 17(4) 329-344.

[11] O. Anwar Bég, Biomimetic propulsion analogies- aerodynamics of small fliers and microscale beating in internal propulsion, *Technical Report, Aero-Mech 3, 94pp, April, University of Salford, Manchester, UK* (2018).

[12] J. Lighthill, *Mathematical Biofluid Dynamics*, SIAM, Philadelphia, USA (1975).

[13] Gheber, L. and Z. Priel (1990). On metachronism in ciliary systems: a model describing the dependence of the metachronal wave properties on the intrinsic ciliary parameters. *Cytoskeleton*, 16(3), 167-181.

[14] Lardner, T. J., Shack, W. J. and E. Waibel (1970). A survey of reproductive biology. *Report to The Pathfinder Fund, Dept. of Mech. Eng., MIT, USA*.

[15] Sanderson, M. J. and M. A. Sleigh (1981). Ciliary activity of cultured rabbit tracheal epithelium: beat pattern and metachrony, *J. Cell Science* 47, 331-347.

[16] Dauptain, A., J. Favier and A. Bottaro (2008). Hydrodynamics of ciliary propulsion, *J. Fluids and Structures* 24, 1156-1165.

[17] Bottier, M., S. Blanchon, G. Pelle, E. Bequignon, D. Isabey, A. Coste and B. Louis (2017). A new index for characterizing microbead motion in a flow induced by ciliary beating: Part I, experimental analysis. *PLoS Computational Biology* 13, e1005605.

[18] K. Ramesh, O. Anwar Bég, D. Tripathi (2018). Cilia-assisted hydromagnetic pumping of biorheological couple stress fluids, *Propulsion and Power Research. **In press***

[19] Ally, J., W. Roa and A. Amirfazli (2008). Use of mucolytics to enhance magnetic particle retention at a model airway surface, *J. Magnetism and Magnetic Materials* 320, 1834-1843.

[20] Kothandapani, M. and J. Prakash (2015). Effect of radiation and magnetic field on peristaltic transport of nanofluids through a porous space in a tapered asymmetric channel, *J. Magnetism and Magnetic Materials,* 378, 152-163.

[21] Hayat, T., F. M. Mahomed and S. Asghar (2005). Peristaltic flow of a magnetohydrodynamic Johnson--Segalman fluid. *Nonlinear Dynamics*, 40, 375-385.

[22] V K Narla, Dharmendra Tripathi, O. Anwar Bég and A Kadir (2018). Modelling transient magnetohydrodynamic peristaltic pumping of electroconductive viscoelastic fluids through a deformable curved channel, *J. Engineering Mathematics. https://doi.org/10.1007/s10665-018-9958-6 (17 pages)*

[23] A. Ramos (2008). Electrohydrodynamic and magneto-hydrodynamic micropumps, In: *Hardt S, Schönfeld F (eds) Microfluidics technologies for miniaturized analysis systems*, Springer, pp 59–116.

[24] O. Anwar Bég (2018). Multi-physical electro-magnetic propulsion fluid dynamics: mathematical modelling and computation, *Mathematical Modeling: Methods, Applications and Research, W. Willis and Seth Sparks (Ed), Chapter 1, 1-88, Nova Science, New York, USA.*

[25] M. Sajid, N. Ali, T. Javed and O. Anwar Bég (2017). Swimming of a singly flagellated micro-organism in a magnetohydrodynamic second order fluid, *J. Mech. Med. Biol.,* 17, 1750009.1-1750009.17.

[26] N. S. Akbar, D. Tripathi, O. Anwar Bég, Z. H. Khan (2016). MHD dissipative flow and heat transfer of Casson fluids due to metachronal wave propulsion of beating cilia with thermal and velocity slip effects under an oblique magnetic field, *Acta Astronautica,* 128, 1-12.

[27] N. S. Akbar, D. Tripathi and O. Anwar Bég (2017). MHD convective heat transfer of nanofluids through a ciliated tube with buoyancy: *A study of nano-particle shape effects, Adv. Powder Technology,* 28 (2) 453-462.

[28] N. S. Akbar, D. Tripathi, Z. H. Khan and O. Anwar Bég (2018). Mathematical modelling of pressure-driven micropolar biological flow due to metachronal wave propulsion of beating cilia, *Mathematical Biosciences* (2018). https://doi.org/10.1016/j.mbs.2018.04.001 (8 pages)

[29] Hoque, M.M., Alam, M.M., Ferdows, M. and O. Anwar Bég (2013). Numerical simulation of Dean number and curvature effects on magneto-biofluid flow through a curved conduit. *Proc. IMechE- Part H; J. Engineering in Medicine,* 227(11), 1155–70.

[30] S. Nadeem and N.S. Akbar (2011). Influence of heat and mass transfer on the peristaltic flow of a Johnson– Segalman fluid in a vertical asymmetric channel with induced MHD, *J. Taiwan Inst. Chem. Eng.* 42: 58–66.

[31] I.J. Rao and K.R. Rajagopal (1999). Some simple flows of a Johnson-Segalman fluid. *Acta Mech.,* 132: 209-219.

[32] Hayat T, Afsar A, Ali N (2005). Peristaltic transport of a Johnson–Segalman fluid in an asymmetric channel. *Math Comput. Mod.,* 47: 380–400.

[33] D. Tripathi, O. Anwar Bég and J. Curiel-Sosa (2014). Homotopy semi-numerical simulation of peristaltic flow of generalized Oldroyd-B fluids with slip effects, *Computer Methods in Biomechanics Biomedical Engineering,* 17(4) 433-442.

[34] D. Tripathi and O. Anwar Bég (2015). Peristaltic transport of Maxwell viscoelastic fluids with a slip condition: Homotopy analysis of gastric transport, *J. Mechanics Medicine Biology, 15 (3)* 1550021.1- 1550021.22.

[35] M. K. Chaube, D. Tripathi, O. Anwar Bég, Shashi Sharma and V.S. Pandey (2015). Peristaltic creeping flow of power law physiological fluids through a non-uniform channel with slip effect, *Applied Bionics and Biomechanics, Volume 2015, Article ID 152802, 10 pages. http://dx.doi.org/10.1155/2015/152802.*

[36] Md. Jashim Uddin, W.A. Khan, A.I.Md. Ismail, O. Anwar Bég (2016). Computational study of three-dimensional stagnation point nanofluid bio-convection flow on a moving surface with anisotropic slip and thermal jump effects, *ASME J. Heat Transfer, 138(10), 104502 (8 pages).*

[37] M.J. Uddin, Y. Alginahi, O. Anwar Bég and M.N. Kabir (2016). Numerical solutions for nonlinear gyrotactic bioconvection in nanofluid saturated porous media with Stefan blowing and multiple slip effects, *Computers and Mathematics with Applications,* 72 (10), 2562-2581.

[38] Lauga, E. and T. R. Powers, (2009). The hydrodynamics of swimming microorganisms. *Reports on Progress in Physics*, 72, 096601.

[39] Nayfeh, A. H. (2008). *Perturbation methods*. John Wiley & Sons.

[40] Hayat T, Javed M, Asghar S (2008). MHD peristaltic motion of Johnson–Segalman fluid in a channel with compliant walls. *Phys Lett A,* 372: 5026–5036.

[41] J. Atencia and D.J. Beebe (2004). Magnetically-driven biomimetic micro-pumping using vortices, *Lab Chip***,** 4, 598-602.

[42] Johnson, M. W. Jr., Segalman, D. (1977). A model for viscoelastic fluid behavior which allows non-affine deformation. *J. Non-Newtonian Fluid Mech*., 2, 255–270.

[43] Hayat T, Wang Y, Siddique AM, Hutter K (2003). Peristaltic motion of Johnson–Segalman fluid in a planar channel. *Math. Prob. Eng.,* 2003: 1–23.

[44] Elshahed M, Haroun MH (2005). Peristaltic transport of Johnson-Segalman fluid under effect of a magnetic field. *Math. Prob. Eng.* 2005: 663–677.

[45] M. Norouzi, M. Davoodi and O. Anwar Bég (2015). An analytical solution for convective heat transfer of viscoelastic flows in rotating curved pipes, *Int. J. Thermal Sciences*, 90, 90-111.